Electrically Driven Robotic Pistons Exploiting Liquid-Vapor Phase Transition for Underwater Applications

Beomchan Kang, Seungseok Lim, Hyunjick Kim, and Wei Dawid Wang

***Abstract*—Soft actuators have shown great potential in underwater applications due to diverse deformations, silent actuation mode, and waterproof features. To accomplish a versatile actuation approach with no environmental disturbances, this study demonstrates an electrically driven robotic piston that combines the advantages of soft robots with those of rigid mechanisms to provide adaptive and robust actuation. The robotic piston was actuated by multiple linearly stacked liquid pouch motors based on the liquid-vapor phase transition. The liquid pouch actuator is filled with low boiling fluid, which is capable of inflating several folds of its initial thickness by Joule heating to a temperature above the boiling point and contracting to the initial state by cooling. Based on the reversible liquid-vapor phase transition of the filled fluid, a series of linearly stacked pouch actuators can inflate and contract, which results in the reciprocating forward and backward movement of the piston rod in contact with them. The performance of liquid pouch actuators and soft robotic pistons was evaluated. The proposed soft robotic piston can be adapted as an electrical machine integrated with other different mechanisms, which was eventually demonstrated in robotic gripper systems and a legged walking robot in the underwater environment.**

***Index Terms*—Soft robotics, phase transition materials, silent actuation, underwater robots.**

I. Introduction

THERE is increasing attention to the extraordinary biodiversity and rich resources of the underwater environment. The need to explore the underwater environment has spurred the development of equipment such as autonomous underwater vehicles and robots [1], [2], [3]. Therefore, various rigid mechanisms have been utilized for a variety of underwater operations, and these traditional mechanisms commonly comprise rigid components like links, gears, and motors [4], [5]. Among these rigid mechanisms, the piston mechanisms are versatile devices for various applications. However, their rigid components, including compressors, valves, and pumps, subject piston mechanisms to bulky and noise issues, and a high risk of lubricant leakage, making them difficult to use in sensitive and unstructured underwater environments.

As an alternate approach to avoid the inherent issues of conventional rigid mechanisms, robotic mechanisms made of soft and compliant materials can achieve safe and adaptive interaction with objects and locomotions in silent mode, providing them greater opportunities for underwater applications [6]. Recent advances in soft underwater robots have been widely investigated based on a diversity of actuation approaches, including hydrogels [7], [8], [9], dielectric elastomer actuators [10], [11], [12], [13], [14], soft fluidic actuators [15], [16], [17], [18], [19], shape memory alloys [20], [21], [22], [23], [24], [25], ionic polymer-metal composite [26], [27], [28], liquid crystal materials [29], [30], magnetic composite elastomers [31], and liquid-vapor phase transition [32], [33], [34], [35]. Although these approaches provide soft actuators with the advantages of lightweight configurations and high flexibility, however, it is difficult for them to provide large deformation and sufficient output force at the same time, and some approaches also require bulky peripheral appendages, such as external magnetic field, electric field, pneumatic control system. Moreover, extended approaches have been demonstrated to scale up actuation deformation and force by assembling multiple soft actuators in stacked configurations [36], [37], [38], [39], [40]. Among various actuation approaches, the liquid pouch motors in a compact configuration can achieve a significant volume change, which enables them to be ideal for the design of soft mechanisms capable of achieving large deformation. In addition, the liquid pouch motors in a stacked configuration will further multiply the achievable deformation, however, this has not yet been demonstrated. On the other hand, the structural stiffness of the stacked soft actuators is low due to the inherent softness of soft actuators, which makes it easy for the stacked assembly to buckle in compression or lose stability when subjected to non-axial external forces [34]. Hence, this study aims to integrate stacked liquid pouch motors with a rigid guide frame to design a stable and robust piston-like soft robotic mechanism.

This study demonstrates the electrically driven soft robotic pistons actuated by multiple linearly stacked liquid pouch actuators based on liquid-vapor phase transition for various underwater applications. The soft robotic piston mainly consists of liquid pouch actuators, a piston rod with a compressed spring, and a

Manuscript received 10 November 2022; accepted 7 February 2023. Date of publication 17 February 2023; date of current version 28 February 2023. This letter was recommended for publication by Associate Editor N. Gravish and Editor Y.-L. Park upon evaluation of the reviewers' comments. This work was supported by the National Research Foundation of Korea (NRF) funded by Korea Government (MSIT) under Grant 2020R1C1C1010295. *(Corresponding author: Wei Dawid Wang.)*

The authors are with the Soft Robotics Lab, Department of Mechanical Engineering, Hanyang University, Seoul 04763, Korea (e-mail: bc6240@hanyang.ac.kr; fsmsmg@hanyang.ac.kr; guswlr3652@hanyang.ac.kr; davidwang@hanyang.ac.kr).

This letter has supplementary downloadable material available at https://doi.org/10.1109/LRA.2023.3246394, provided by the authors.

Digital Object Identifier 10.1109/LRA.2023.3246394

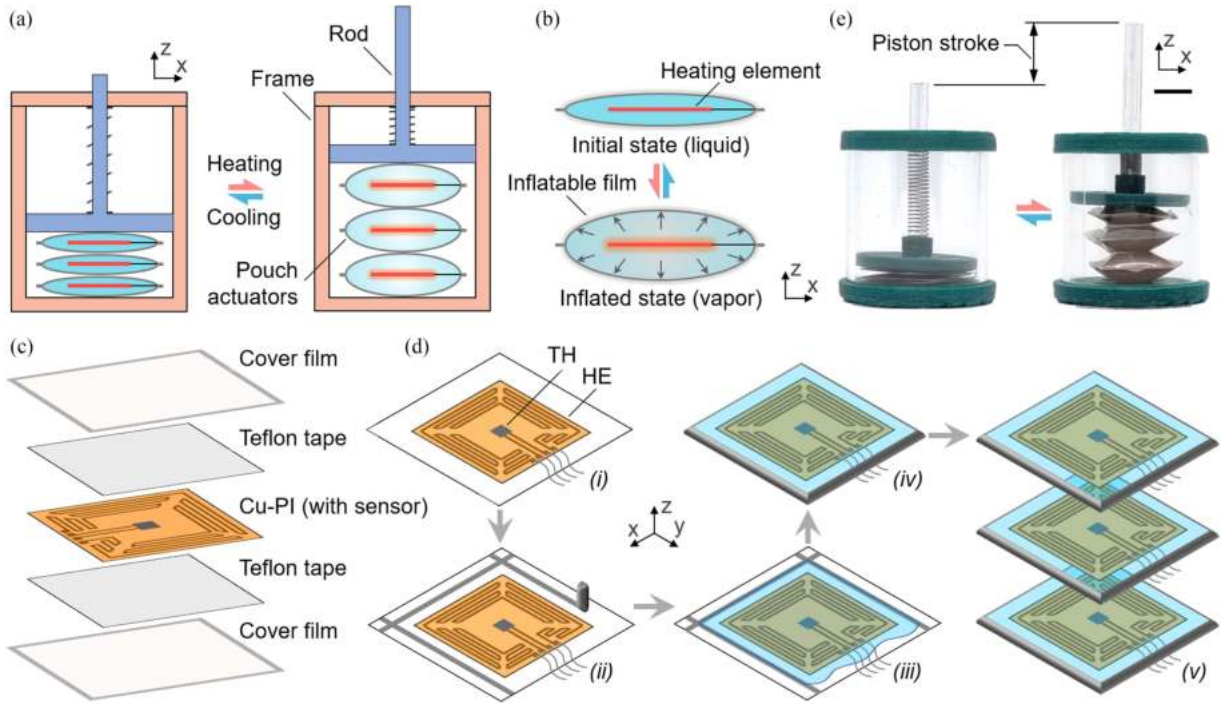

Fig. 1. **Working principle, design, and fabrication of pouch actuator-based soft robotic piston.** (a) Working principle of the robotic piston based on linearly stacked soft pouch actuators. The expansion and contraction of multiple stacked pouch actuators enable the piston rod to move up and down, respectively. (b) Working principle of a single pouch actuator filled with low boiling point engineered fluid. Through the phase change of the filled fluid, the pouch expands when heated above the boiling temperature via Joule heating, or contracts via free cooling. (c) Prototype of a soft robotic piston before and after actuation. The scaler bar is 20 mm. (d) Main components of a pouch actuator. The heating element is made of copper-polyimide (Cu-PI) film with thin copper traces on a polyimide film formed by etching. A temperature sensor (indicated by the black square) to measure the temperature inside the pouch is soldered to the center of the heating element. (e) The fabrication process of linearly stacked soft pouch actuators. TH: thermistor. HE: heating element.

frame to hold all the components. Each liquid pouch actuator is made from a flexible and inextensible shell that is filled with low-boiling fluid and embedded with a heating element. Joule heating the heating element enables the inflation of the pouch due to liquid to vapor phase transition, and free cooling will contract the inflated pouch due to the inverse phase transition. The compressed spring allows the piston rod to fit against the pouch actuators without separation, allowing the rod to move up and down as the pouch actuators inflate and contract. That is, the displacement of the rod (i.e., the stroke of the piston), equals the total inflated deformation of the pouch actuators. Moreover, the soft robotic piston can serve as an electrical machine, which can be integrated with other mechanisms that can convert electrical energy into mechanical work for different robotic applications. As demonstrations, the soft robotic pistons were eventually applied to different designs, including robotic gripper systems and a legged, walking robot in the underwater environment.

II. Concept and Fabrication

The proposed soft robotic piston mainly consists of a set of linearly stacked liquid pouch actuators, a piston rod with a compressed spring, and a frame to hold all components (Fig. 1(a)). The compressed spring is used to keep the piston rod in constant contact with the pouch actuators, which enables the inflated deformation of the pouch actuators to equal the stroke of the piston. The liquid pouch actuator is an inflated but inelastic pouch filled with a non-toxic fluid of low boiling temperature of 34 °C (Novec 7000, 3M) as the phase-transition material. This boiling point was chosen because it is much lower than that of water and higher than most underwater temperatures. Fig. 1(b) shows the working principle of the liquid pouch actuator. Joule heating the built-in resistive heating element to a temperature above the boiling point enables the filled fluid to change from the liquid state to the vapor state causing inflated deformation, while free cooling enables the reverse change from vapor to liquid to induce contracted deformation. The constitutions of the pouch are shown in Fig. 1(c). The aluminum oxide-coated plastic film (AlOx-PET, FlexFilms) with a thickness of 12 um is used as the shell due to its properties of flexibility, heat sealability, and high gas barrier. The heating element, with a resistance of around 4.8 Ω, is made of the copper-polyimide film with filamentary serpentine copper traces on a polyimide film formed by etching. A thermistor (TTF-103, TKS) that measures the temperature inside the pouch is soldered to the center of the heating element. A layer of Teflon tape, used as the heat-resistant layer, is pasted to the inner side of the shell film to prevent overheating when in direct contact with the heating element. Fig. 1(d) illustrates the main fabrication process to construct the stacked liquid pouch actuators. First, the constituent materials of the pouch are stacked together and heat-sealed into a pouch shape remaining one side open to fill it with the fluid of around 0.2 μl. After filling, the pouches were sealed completely to form the pouch actuator with

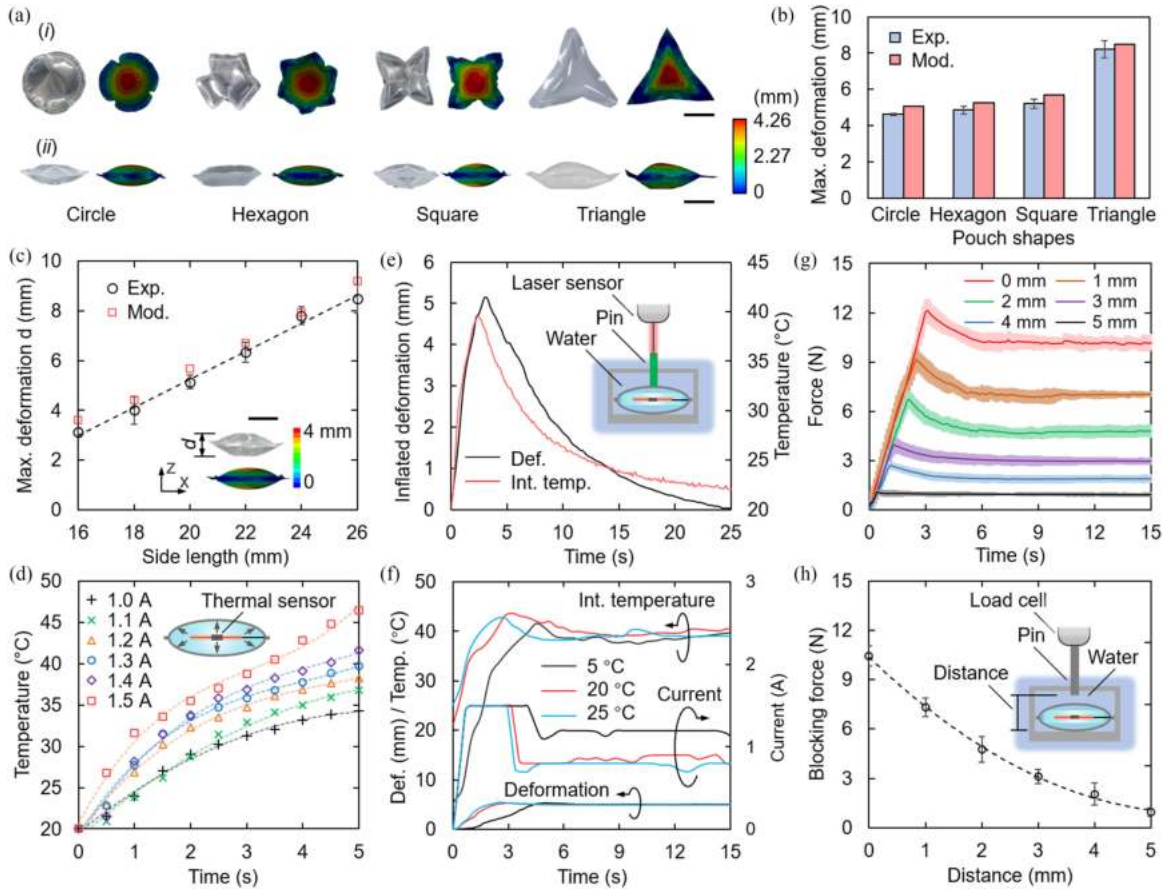

Fig. 2. **Performance evaluations of the soft pouch actuator.** (a) Effect of the shape of the soft pouch actuator on its maximum inflated deformation. Top view (*i*) and side view (*ii*) of both the experimental and modeling results of the fully inflated pouches in the shapes of circle, hexagon, square, and triangle, respectively. (b) Comparison of the maximum inflated deformation of different pouches. (c) The maximum inflated deformation of the square pouches with different size lengths. The inset shows the experimental and modeling results of a fully inflated square pouch with a side length of 20 mm. (d) The internal temperature of the pouch changes with time under different applied currents. The temperature was measured using the embedded temperature sensor soldered to the center of the heating element. (e) The inflation and contraction of the pouch actuator with the temperature change at an applied electrical current of 1.5 A for 3 s. Inset shows the experimental setup. (f) The variation of the inflated deformation, the internal temperature of the pouch actuator, and electrical currents under the PID temperature control at different ambient temperatures of 5 °C, 20 °C, and 25 °C in the water. (g) Blocking forces of the pouch actuator at different deformations over time. (h) The stabilized blocking forces of the pouch actuator at different deformations. Inset shows the experimental setup. Scale bars: 10 mm.

a total weight of around 1 g. Last, multiple fabricated pouch actuators were aligned and stacked. To further construct the robotic piston, an acrylic cylinder (with an inner diameter of 34 mm and a wall thickness of 2 mm) with top and bottom caps was used as the sleeve to place the stacked soft pouch actuators and a spring-loaded acrylic bar (with an outer diameter of 5 mm and a length of 50 mm) with a round base was used as a piston rod. A soft robotic piston consisting of three pouch actuators is demonstrated in Fig. 1(e), where synchronous inflation and contraction of the pouch actuators lead to the forward and backward strokes of the piston, respectively. The repetitive phase change of filled fluid in the pouches results in a reciprocating linear motion of the piston rod.

III. Results

A. Determining the Pouch Dimensions

Experiments were first conducted to analyze the effect of the geometric feature on the maximum inflated deformation of the pouch actuator. To do so, three pouch actuators of the same area but different shapes of circle, hexagon, square, and triangle were fabricated, respectively. The maximum inflated deformation perpendicular to the sealing plane was measured for each pouch after immersing the pouch in hot water of 50 °C for instant expansion. The experimental results were also verified by using finite element simulation. To do so, Abaqus/Explicit (Abaqus, version 6.13) is used to solve the problem of shell structures subjected to internal pressures, along with the 3D shells meshed using the S4R element, which is most suitable for large deformation analysis (Fig. 2(a)). Results show that the triangle pouch actuator can generate more wrinkles on the actuator surface resulting in a larger inflated deformation than others (Fig. 2(b)). However, the pouch in a triangle shape was excluded due to its long side length and lack of stability of stacking, and the one in a square shape with the largest amount of deformation among other shapes was selected in the following designs. Experiments were further conducted to evaluate the side length on the maximum inflated deformation of the square pouch actuator. The side length varied from 16 mm to 26 mm in 2 mm increments, and both experimental and modeling results

of maximum inflated deformation are shown in Fig. 2(c). Results show that the maximum inflated deformation of the pouch approximately increases linearly with the increase of side length, and a side length of 20 mm with a maximum inflated deformation of 5.1 mm is selected for the follow-up experiments.

B. Heating Capacity of the Heating Element

Joule heating the resistive heating element is used to trigger the phase transition from the liquid state to the vapor state of the filled fluid. Experiments were conducted to measure the temperature change of the heating element at different applied currents ranging from 1.0 A to 1.5 A in 0.1 A increments. The internal temperature of the pouch was measured using the embedded thermistor soldered to the center of the heating element. Results show that a higher current leads to a faster heating speed and the recorded peak temperatures at the third second were 31.3, 32.9, 34.7, 35.8, 36.9, and 38.9 °C for 1.0, 1.1, 1.2, 1.3, 1.4, and 1.5 A, respectively (Fig. 2(d)). The control strategy for the pouch actuator is achieved by rapidly heating via a high current at the beginning to bring the temperature inside the pouch above the boiling point and then reducing the current to maintain the internal temperature at 40 °C. Hence, the current of 1.5 A capable of heating up to around 40 °C in 3 s is chosen as the initial input current to ensure fast inflation of the pouch actuator.

C. Controlling Deformation of Soft Pouch Actuator

The inflated deformation and temperature change inside the pouch actuator were measured with a current of 1.5 A applied for 3 s at a water temperature of 20 °C (Fig. 2(e), Movie S1). It can be seen that the pouch actuator closely follows the internal temperature change and requires around 3 s to achieve the maximum deformation and more than 20 s to contract to the initial configuration. The soft pouch actuator takes much more time to contract than to inflate since most of the contracting time is spent in restoring the initial stage of deformation.

The surrounding temperatures will also affect the deformation of the pouch, where a low surrounding temperature requires a higher current or longer time to inflate the pouch actuators to their maximum deformation, and a high temperature requires a low current or short time. To avoid these effects, a PID control strategy implemented by a microcontroller (MCU, ATmega328P, Microchip Technology) was introduced into the soft pouch actuators to control its internal temperature preventing overheating and minimizing energy consumption. The set target temperature (T_0) is transmitted from the host computer to MCU. After which, MCU consistently reads the analog signal from the thermistor inside the soft pouch actuator and converts it to the present temperature value (T_1). The output control signal, which is corresponded to the electrical current, is calculated by using the deviation between T_0 and T_1 through the PID algorithm. In addition, to prevent overshooting and to converge stably to the desired temperature, the set output control current is restricted between an upper and lower limit, and the allowable current intensity is automatically adjusted according to the ambient water temperature. Thus, the host computer can control the current intensity which is provided to the DC power supply (RD6012-KA, Daqnet) in real time.

Experiments were conducted at three different water temperatures of 5, 20, and 25 °C. The results show that the PID control enables the pouch actuator to maintain its maximum inflated deformation by keeping the internal temperature of the pouch actuator at the targeted temperature of 40 °C. The maintained temperature was achieved by automatically adjusting the magnitude of the input current to the heating element in real-time, where the current started from 1.5 A to a gradually steady current with small fluctuations of around 1.14, 0.86, and 0.77 A (with corresponding power of 5.7, 4.3, and 3.5 W) for the three different water temperatures, respectively (Fig. 2(f)).

D. Actuation Force of Soft Pouch Actuator

The actuation force generated by the pouch actuator was also measured. This experiment was conducted by fixing the pouch actuator to the bottom of a water container with the top surface of the pouch actuator in close contact with the rod structure secured to a load cell. The distance between the top surface of the pouch actuator and the bottom end of the rod structure was adjusted from 0 mm to 5 mm with 1 mm increments. For each distance, the pouch actuator was actuated using the proposed PID control strategy and the blocking force was measured and recorded (Fig. 2(g)). The results show that, except for a rapid increase at the beginning, the force can be maintained at an output value. The maintained output forces are also described in Fig. 2(h) and results show that the force decreases with an increasing distance where the force changes from 10.4 N at 0 mm to 0.9 N at 5 mm. The energy density of the soft pouch actuator, with a mass of 1 g and initial thickness of 1 mm, is 22.7 J kg^{-1} (i.e., the quotient of the area under the curve and mass), while the inflated deformation of the actuator increased to more than 5 times.

E. Performances Evaluation of the Robotic Piston

A soft robotic piston composed of five identical soft pouch actuators was constructed and it can lift a weight of 50 g with a piston stroke of 25 mm (Fig. 3(a)). Each pouch actuator can be controlled individually, thereby controlling a different number of working pouch actuators, allowing it to achieve different strokes of the piston. Therefore, controlling one to five working pouches respectively under the same conditions can obtain a stroke equal to the amount of deformation of a single working pouch multiplied by the number of working pouches (Fig. 3(b), Movie S2). At 20 °C, each pouch actuator was actuated by applying a current of 1.5 A for 3 s to allow the actuator to be fully inflated to advance the piston rod, and then the current was cut off resulting in the contraction of the actuator to retract the rod. The piston strokes were measured as around 5.0, 9.6, 15.1, 20, and 25.3 mm for one, two, three, four, and five working pouch actuators, respectively.

The PID controller is introduced to control the internal temperature of the pouch actuator to enable the total deformation of the constituent pouch actuators (i.e., the advanced distance of the piston rod), to be steadily maintained at a certain magnitude.

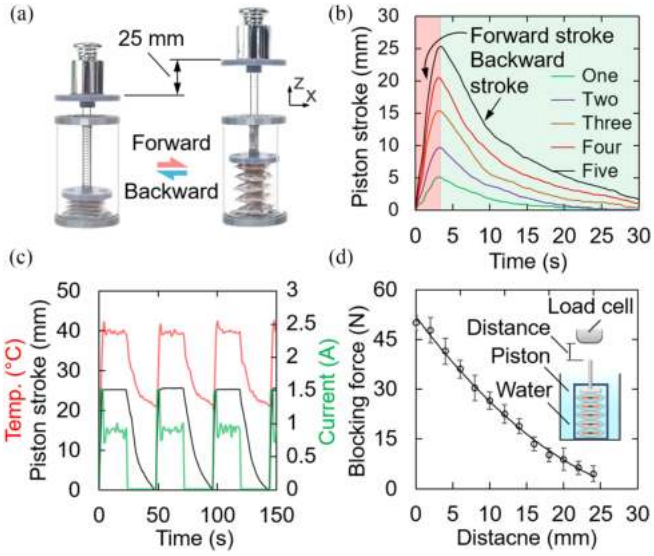

Fig. 3. **Performance evaluations of the soft robotic piston.** (a) A prototype of the soft robotic piston actuated by five stacked soft pouch actuators lifting a weight of 50 g with a stroke of 25 mm. Scale bar: 20 mm. (b) Strokes of the soft robotic piston with different numbers of working soft pouch actuators. (c) The cyclic stroke under the PID temperature control over five cycles. For each cycle, the piston rod with a forward stroke of 25 mm is maintained for 20 s. (d) The blocking force of the robotic piston consisting of five pouch actuators under a varied distance between the load cell and the end of the piston rod. Inset shows the experimental setup.

The PID controller is accomplished where a current of 1.5 A was first applied for rapid heating, then the current was automatically adjusted to maintain the internal temperature at 40 °C for the desired time interval, and after that, the current was cut off for cooling. Fig. 3(c) shows the periodic actuation of the robotic piston where for each period the piston rod rapidly advances 25 mm, then maintains the position for 20 s, and after that retracts to the initial position.

The blocking force of the piston was also measured to evaluate the load capability of the robotic piston. This force was measured by holding one end fixed and adjusting the distance between the end of the rod and the load cell. The composed pouch actuators of the robotic piston were synchronously actuated to advance the rod to contact the load cell, and the steady output force was recorded as the blocking force (Fig. 3(d)). Results show that the blocking force decreases with increasing distance where the force changes from 51.5 N at 0 mm to 5.7 N at 24 mm.

F. Soft Robotic Grippers

The soft robotic piston can be adapted as the power source for a variety of different mechanisms with different applications. The soft robotic piston is introduced to the design of gripping systems based on tendon-driven mechanisms. A soft gripper system consisting of five identical flexible petaloid soft fingers is first designed to be capable of grasping soft and fragile objects. The five fingers are installed to a hub structure placed at the bottom of the robot piston and the angle between each finger and the hub is 45°. Each finger (with a length of 150 mm) is controlled by an individual wire where a nylon wire is then passed through the predesigned holes on the inner side of each finger and holes on the caps of the robotic piston and finally fixed to the fixer structure at the end of the piston rod (Fig. 4(a)). The forward stroke of the piston pulls the wires to bend all the soft fingers to achieve a completely closed configuration to capture objects (Fig. 4(b)). The backward stroke will release the wire to open the gripper to release the objects.

The grasping force was measured by firmly installing the gripper to the same load cell to measure the force generated by the gripper on a fixed object during an upward motion. The piston was fully actuated to enable the gripper to grasp a fixed ball with a diameter of 100 mm, while the upward movement of the load cell moves the gripper from caging to detaching the ball. The pulling force is recorded as the grasping force and a maximum force of 0.7 N is observed (Fig. 4(c)). The softness and harmlessness enable the soft gripper to be used to catch delicate or spiny marine creatures including jellyfish, sea urchins, and fish (Fig. 4(d) and Movie S3). At 20 °C, the gripper can switch from an open state to a closed state for caging objects within 3 s. Moreover, the gripper can perform a series of motions, including grasping, moving, and releasing the objects.

Another application of underwater exploration is the collection of mineral resources such as manganese nodules. To accurately collect these unstructured and heavy objects, the second gripper is designed where the five soft fingers were replaced by three rigid hinged fingers (Fig. 4(e)). Each finger (with a length of 75 mm) consists of three segments connected using pin joints, and the three fingers are connected by one wire to achieve an underactuated gripper mechanism (Fig. 4(f)), allowing all fingers to be synergistically adapted and conformed to the shape of the targets. The installed angle between each finger and the hub is 60°. The wire path is directed inside the finger segments using dedicated holes without interfering with the grasped object. Besides, a spring is installed between two adjacent finger segments to provide restoring force to return the bent finger to its straight state. The grasping force was also measured in the same way as mentioned in the previous experiments to grip a fixed ball with a diameter of 50 mm (Fig. 4(g)), and the measured maximum grasping force is about 6 N, which is approximately nine-fold that of the gripper. The gripper is then used to grip a marine stone (380 g) with an unstructured shape (Fig. 4(h)). This test also showed that utilizing the underactuated gripper mechanism can maintain a stable grasp on an unstructured shape due to the adaptive contact between the fingers and the object. Further experiments were also conducted to collect marine sedimentary waste (Movie S4).

G. Walking Robot

To explore further applications, the proposed piston is then introduced to the design of a four-legged walking robot. The walking robot consists of two horizontal pistons with a length of 50 mm as the left and right two body parts, four vertical pistons with a length of 35 mm as the four legs, and auxiliary rigid structures hold these pistons in place (Fig. 5(a)). The left and right two body parts are connected through two parallel links to form a single robot platform. Moreover, to avoid the

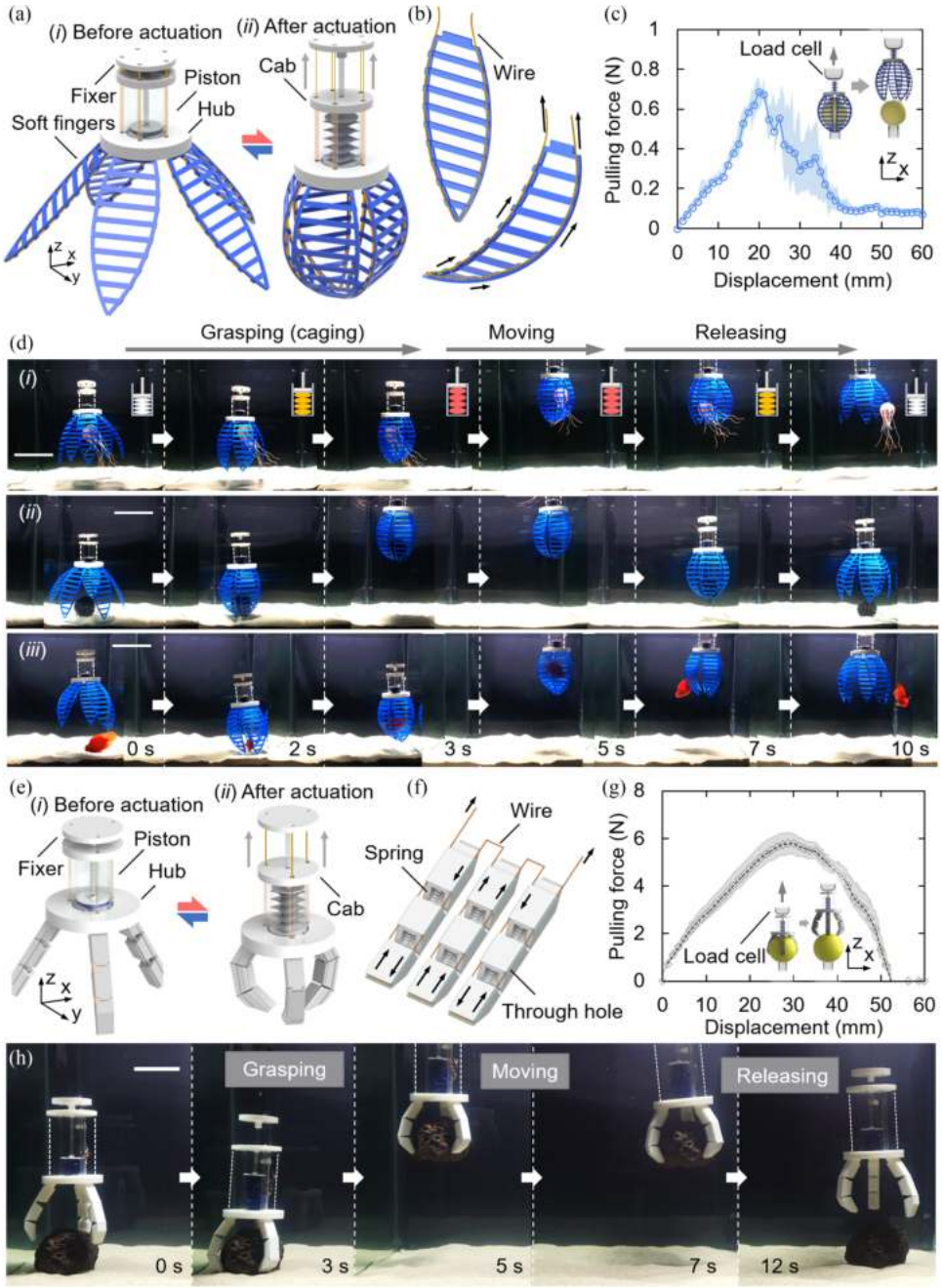

Fig. 4. Application to gripping systems. (a) Configurations of the wire-driven soft gripper system composed of five petaloid soft fingers before and after actuation. (b) The wire path of each finger. (c) Pulling force of the soft gripper from caging the object (a fixed ball with a diameter of 100 mm) to their separation. The inset shows the schematic of the experiment setup. (d) The soft gripper is used to grasp delicate or spiny marine creatures by caging them inside, including jellyfish, sea urchins, and fish (from top to bottom). Insets show the diagrams of different states of the piston, where white, red, and yellow indicate unactuated, being actuated, and fully actuated pistons, respectively. (e) Configurations of the gripper composed of three identical rigid fingers. (f) Wire path for the finger mechanism. (g) Pulling force of the rigid gripper from caging the object (a fixed ball with a diameter of 50 mm) to their separation. The inset shows the schematic of the experiment setup. (h) The rigid gripper is used to collect a marine stone weighing 380 g. Scale bars: 50 mm.

inability of the leg pistons to lift the entire robot structure due to insufficient output force, the leg pistons were modified to an actuate-to-pull design, and a cap is attached to each piston rod as the foot, so the leg steps on the ground when resting and lifts when operating the piston.

Each piston can be independently operated to enable the robot to be capable of achieving walking motion with desired gaits. Similar to the locomotion of tetrapod animals, each stride of the linear motion of the robot was implemented in the following steps: (i) lifting the front leg at one side of the robot, (ii) advancing the rod of the body piston at the same side to push the front leg forward, (iii) lifting the rear leg at the same side, (iv) retracting the rod of body piston to pull the real leg forward, (v) putting the rear leg down, and (vi) repeating the actions

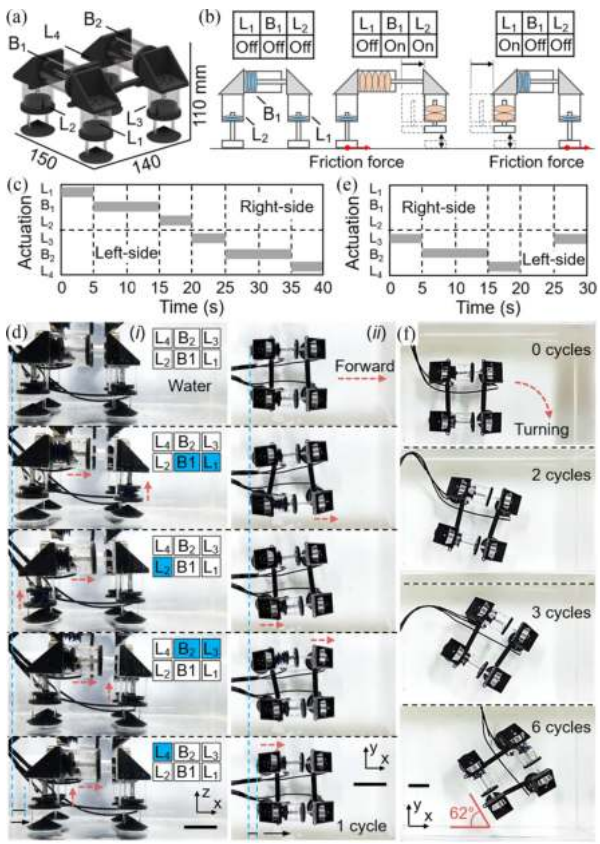

Fig. 5. Application to a walking robot. (a) Schematic of the walking robot with its main components and overall dimensions. The walking robot comprises four leg pistons (L1 to L4) and two body pistons (B1 and B2). (b) Schematic diagrams show the actuation sequences of composed pistons for locomotion. (c) Actuation patterns for linear motion. (d) Photographs show the sequences of linear motion. The blue boxes in the upper-right corner of each figure indicate that the pistons are fully actuated, and the white boxes indicate that the piston is unactuated. (e) Actuation patterns for a right-turning motion. (f) Photographs show the sequences of the right-turning motion. Scale bars: 50 mm.

mentioned above for the other body side. The experiments were conducted at 20 °C, and the actuating and unactuating times for each piston were determined as 5 s and 10 s. The actuation sequence used to generate the forward motion consisting of one stride is illustrated in Fig. 5(c), with the running time for each stride being 40 s. The robot at different steps of this locomotion is shown in Fig. 5(d) (Movie S5). The persistence of the motion of the robot was tested by continuous motion for an hour, and the final speed was approximately 0.42 mm/s, and 0.22 body length per stride, where the body length is 150 mm. Moreover, the robot can also perform a straight walking motion in the opposite direction on uneven sand surfaces by applying the inverse actuation steps. Turning motion can be achieved by actuating only one side of the robot body, and the actuation sequence with a period of 25 s used to generate the right turning motion is illustrated in Fig. 5(e). The robot at different steps of this turning locomotion is shown in Fig. 5(f) (Movie S5). The turning speed of the robot calculated from the recorded video is approximately 0.27° per second, and 10.6° per stride.

IV. Limitation & Future Work

A. Actuation Speed

The actuation period of the square pouch with a side length of 20 mm is around 20 s. But there are several ways to achieve faster actuation. One solution is to make a smaller pouch. Our preliminary experiments show that a square pouch with a side length of 5 mm can achieve less deformation, but a faster actuation cycle of a few seconds. Therefore, the actuation speed and deformation of the overall mechanism can be met by mechanically arranging multiple small pouches in different ways. In addition, future works on a single liquid pouch motor will be optimizing the structure design, reducing power consumption, and improving the actuation frequencies.

B. Sealability and Permeability

Even though the used low boiling fluid is typically known as an environmentally friendly material, it is likely to harm underwater environments. Although the leakage from the seal line of the pouch has not founded during the experiments, the pouch should be prevented from being damaged due to overheating, so as to avoid liquid leakage. In addition, the permeability of the liquid pouch actuator was measured, and results show that there is a loss of fluid or vapor of around 0% and less than 2% in the liquid and vapor states for 14 consecutive days, respectively. Considering that the amount of fluid injected in the pouch is small, one can say that the current design of the liquid pouch can minimize the potential risk of leakage of sealed fluid. Further work should be conducted to determine whether the used low-boiling fluid is hazardous in the underwater environment.

V. Conclusion

In summary, this study demonstrates an electrically actuated soft robotic piston based on liquid-vapor phase transition for underwater applications including gripping mechanisms and a quadruped walking platform. It is worth mentioning that the proposed robotic piston mechanism is not limited to the demonstrated applications and could be widely used as a general electrical machine for more application contexts to achieve the desired output through different designs. Compared to the mechanical piston-like system with a rigid mechanism, the soft robotic piston proposed in this study offers several promising benefits. First, the proposed piston mechanism based on liquid-vapor phase transition can eliminate the disadvantages of traditional motor systems, thus providing quiet and silent operations without disturbances to the surroundings for usage in sensitive, underwater environments. Second, the stroke of the piston can be customized by constructing the piston through multiple pouches and then choosing to actuate different numbers of pouches to achieve strokes with different magnitudes. In addition, all components of the soft robotic piston are waterproof enabling the robotic piston to be well used in water. Furthermore, the proposed robotic piston combines the advantages of soft robots and rigid mechanisms to provide safe interaction with objects and robust actuation even without additional sensing.

REFERENCES

[1] T. R. McClanahan, M. J. Marnane, J. E. Cinner, and W. E. Kiene, "A comparison of marine protected areas and alternative approaches to coral-reef management," *Curr. Biol.*, vol. 16, no. 14, pp. 1408–1413, 2006, doi: 10.1016/j.cub.2006.05.062.

[2] W. W. L. Cheung et al., "Marine resources to climate change," *ICES J. Mar. Sci.*, vol. 73, pp. 1283–1296, 2016.

[3] N. Palomeras, N. Hurtos, E. Vidal, and M. Carreras, "Autonomous exploration of complex underwater environments using a probabilistic next-best-view planner," *IEEE Robot. Autom. Lett.*, vol. 4, no. 2, pp. 1619–1625, Apr. 2019, doi: 10.1109/LRA.2019.2896759.

[4] G. Picardi, M. Chellapurath, S. Iacoponi, S. Stefanni, C. Laschi, and M. Calisti, "Bioinspired underwater legged robot for seabed exploration with low environmental disturbance," *Sci. Robot.*, vol. 5, no. 42, 2020, Art. no. eaaz1012.

[5] A. Sahoo, S. K. Dwivedy, and P. S. Robi, "Advancements in the field of autonomous underwater vehicle," *Ocean Eng.*, vol. 181. pp. 145–160, 2019, doi: 10.1016/j.oceaneng.2019.04.011.

[6] S. Aracri et al., "Soft robots for ocean exploration and offshore operations: A perspective," *Soft Robot,* vol. 8, no. 6, pp. 625–639, 2021, doi: 10.1089/soro.2020.0011.

[7] H. Yuk, S. Lin, C. Ma, M. Takaffoli, N. X. Fang, and X. Zhao, "Hydraulic hydrogel actuators and robots optically and sonically camouflaged in water," *Nature Commun.*, vol. 8, 2017, Art. no. 14230, doi: 10.1038/ncomms14230.

[8] S. L. Xiang, Y. X. Su, H. Yin, C. Li, and M. Q. Zhu, "Visible-light-driven isotropic hydrogels as anisotropic underwater actuators," *Nano Energy*, vol. 85, 2021, Art. no. 105965, doi: 10.1016/j.nanoen.2021.105965.

[9] L. Migliorini, T. Santaniello, Y. Yan, C. Lenardi, and P. Milani, "Low-voltage electrically driven homeostatic hydrogel-based actuators for underwater soft robotics," *Sensors Actuators, B Chem*, vol. 228, pp. 758–766, 2016, doi: 10.1016/j.snb.2016.01.110.

[10] C. Christianson, N. N. Goldberg, D. D. Deheyn, S. Cai, and M. T. Tolley, "Translucent soft robots driven by frameless fluid electrode dielectric elastomer actuators," *Sci. Robot.*, vol. 3, 2018, Art. no. eaat1893, doi: 10.1126/scirobotics.aat1893.

[11] J. Shintake, V. Cacucciolo, H. Shea, and D. Floreano, "Soft biomimetic fish robot made of dielectric elastomer actuators," *Soft Robot*, vol. 5, no. 4, pp. 466–474, 2018, doi: 10.1089/soro.2017.0062.

[12] Z. Zhang et al., "Global vision-based formation control of soft robotic fish swarm," *Soft Robot*, vol. 8, no. 3, pp. 310–318, 2021, doi: 10.1089/soro.2019.0174.

[13] G. Li et al., "Self-powered soft robot in the Mariana Trench," *Nature*, vol. 591, no. 7848, pp. 66–71, 2021, doi: 10.1038/s41586-020-03153-z.

[14] C. Christianson et al., "Jellyfish-inspired soft robot driven by fluid electrode dielectric organic robotic actuators," *Front. Robot. AI*, vol. 6, 2019, Art. no. 126, doi: 10.3389/frobt.2019.00126.

[15] N. R. Sinatra, C. B. Teeple, D. M. Vogt, K. K. Parker, D. F. Gruber, and R. J. Wood, "Ultragentle manipulation of delicate structures using a soft robotic gripper," *Sci. Robot.*, vol. 4, no. 33, 2019, Art. no. eaax5425, doi: 10.1126/scirobotics.aax5425.

[16] J. Liu, S. Iacoponi, C. Laschi, L. Wen, and M. Calisti, "Underwater mobile manipulation: A soft arm on a benthic legged robot," *IEEE Robot. Autom. Mag.*, vol. 27, no. 4, pp. 12–26, Dec. 2020, doi: 10.1109/MRA.2020.3024001.

[17] R. K. Katzschmann, J. DelPreto, R. MacCurdy, and D. Rus, "Exploration of underwater life with an acoustically controlled soft robotic fish," *Sci. Robot.*, vol. 3, no. 16, 2018, Art. no. eaar3449, doi: 10.1126/scirobotics.aar3449.

[18] K. C. Galloway et al., "Soft robotic grippers for biological sampling on deep reefs," *Soft Robot*, vol. 3, no. 1, pp. 23–33, 2016, doi: 10.1089/soro.2015.0019.

[19] J. Frame, N. Lopez, O. Curet, and E. D. Engeberg, "Thrust force characterization of free-swimming soft robotic jellyfish," *Bioinspiration Biomimetics*, vol. 13, no. 6, 2018, Art. no. 64001, doi: 10.1088/1748-3190/aadcb3.

[20] Z. Wang, G. Hang, J. Li, Y. Wang, and K. Xiao, "A micro-robot fish with embedded SMA wire actuated flexible biomimetic fin," *Sensors Actuators A, Phys.,* vol. 144, no. 2, pp. 354–360, 2008, doi: 10.1016/j.sna.2008.02.013.

[21] W. Wang, N. G. Kim, H. Rodrigue, and S. H. Ahn, "Modular assembly of soft deployable structures and robots_SI," *Mater. Horiz.*, vol. 4, no. 3, pp. 367–376, 2017, doi: 10.1039/c6mh00550k.

[22] Y. Almubarak, M. Punnoose, N. X. Maly, A. Hamidi, and Y. Tadesse, "KryptoJelly: A jellyfish robot with confined, adjustable pre-stress, and easily replaceable shape memory alloy NiTi actuators," *Smart Mater. Struct.*, vol. 29, no. 7, 2020, Art. no. 75011, doi: 10.1088/1361-665X/ab859d.

[23] S. H. Song et al., "Turtle mimetic soft robot with two swimming gaits," *Bioinspiration Biomimetics*, vol. 11, no. 3, 2016, Art. no. 36010, doi: 10.1088/1748-3190/11/3/036010.

[24] W. Coral, C. Rossi, O. M. Curet, and D. Castro, "Design and assessment of a flexible fish robot actuated by shape memory alloys," *Bioinspiration Biomimetics*, vol. 13, no. 5, 2018, Art. no. 56009, doi: 10.1088/1748-3190/aad0ae.

[25] J. Hwang and W. D. Wang, "Shape memory alloy-based soft amphibious robot capable of seal-inspired locomotion," *Adv. Mater. Technol.*, vol. 7, Feb. 2022, Art. no. 2101153, doi: 10.1002/admt.202101153.

[26] Q. Shen et al., "Basic design of a biomimetic underwater soft robot with switchable swimming modes and programmable artificial muscles," *Smart Mater. Struct.*, vol. 29, 2020, Art. no. 35038, doi: 10.1088/1361-665X/ab6fe8.

[27] Z. Chen, T. I. Um, and H. Bart-Smith, "A novel fabrication of ionic polymer-metal composite membrane actuator capable of 3-dimensional kinematic motions," *Sensors Actuators, A Phys.*, vol. 168, pp. 131–139, 2011, doi: 10.1016/j.sna.2011.02.034.

[28] J. J. Hubbard, M. Fleming, V. Palmre, D. Pugal, K. J. Kim, and K. K. Leang, "Monolithic IPMC fins for propulsion and maneuvering in bioinspired underwater robotics," *IEEE J. Ocean. Eng.*, vol. 39, no. 3, pp. 540–551, Jul. 2014, doi: 10.1109/JOE.2013.2259318.

[29] H. Shahsavan et al., "Bioinspired underwater locomotion of light-driven liquid crystal gels," *Proc. Nat. Acad. Sci. USA*, vol. 117, no. 10, pp. 5125–5133, 2020, doi: 10.1073/pnas.1917952117.

[30] H. Tian, Z. Wang, Y. Chen, J. Shao, T. Gao, and S. Cai, "Polydopamine-coated main-chain liquid crystal elastomer as optically driven artificial muscle," *ACS Appl. Mater. Interfaces*, vol. 10, no. 9, pp. 8307–8316, 2018, doi: 10.1021/acsami.8b00639.

[31] Z. Ren, W. Hu, X. Dong, and M. Sitti, "Multi-functional soft-bodied jellyfish-like swimming," *Nature Commun.*, vol. 10, no. 1, 2019, Art. no. 2703, doi: 10.1038/s41467-019-10549-7.

[32] K. Narumi et al., "Liquid pouch motors: Printable planar actuators driven by liquid-to-gas phase change for shape-changing interfaces," *IEEE Robot. Autom. Lett.*, vol. 5, no. 3, pp. 3915–3922, Jul. 2020, doi: 10.1109/LRA.2020.2983681.

[33] B. Kang, Y. Lee, T. Piao, Z. Ding, and W. D. Wang, "Robotic soft swim bladder using liquid-vapor phase transition," *Mater. Horiz.*, vol. 8, no. 3, pp. 939–947, 2021, doi: 10.1039/d0mh01788d.

[34] M. Boyvat, D. M. Vogt, and R. J. Wood, "Ultrastrong and high-stroke wireless soft actuators through liquid–gas phase change," *Adv. Mater. Technol.*, vol. 4, no. 2, pp. 1–6, 2019, doi: 10.1002/admt.201800381.

[35] A. Miriyev, K. Stack, and H. Lipson, "Soft material for soft actuators," *Nature Commun.*, vol. 8, no. 1, pp. 1–8, 2017, doi: 10.1038/s41467-017-00685-3.

[36] N. Kellaris, V. Gopaluni Venkata, G. M. Smith, S. K. Mitchell, and C. Keplinger, "Peano-HASEL actuators: Muscle-mimetic, electrohydraulic transducers that linearly contract on activation," *Sci. Robot.*, vol. 3, no. 14, 2018, Art. no. eaar3276, doi: 10.1126/scirobotics.aar3276.

[37] B. H. Lee, N. Oh, and H. Rodrigue, "Expanding pouch motor patterns for programmable soft bending actuation: Enabling soft robotic system adaptations," *IEEE Robot. Autom. Mag.*, vol. 27, no. 4, pp. 65–74, Dec. 2020.

[38] S. Li, D. M. Vogt, N. W. Bartlett, D. Rus, and R. J. Wood, "Tension pistons: Amplifying piston force using fluid-induced tension in flexible materials," *Adv. Funct. Mater.*, vol. 29, no. 30, 2019, Art. no. 1901419, doi: 10.1002/adfm.201901419.

[39] R. Niiyama, X. Sun, C. Sung, B. An, D. Rus, and S. Kim, "Pouch motors: Printable soft actuators integrated with computational design," *Soft Robot*, vol. 2, no. 2, pp. 59–70, 2015, doi: 10.1089/soro.2014.0023.

[40] M. Duduta, E. Hajiesmaili, H. Zhao, R. J. Wood, and D. R. Clarke, "Realizing the potential of dielectric elastomer artificial muscles," *Proc. Nat. Acad. Sci. USA*, vol. 116, no. 7, pp. 2476–2481, 2019, doi: 10.1073/pnas.1815053116.